Ann. Geophysicae 16, 189–196 (1998)

Annales Geophysicae

The role of water-vapour photodissociation on the formation of a deep minimum in mesopause ozone

I. M. Vardavas[1], **J. H. Carver**[2], **F. W. Taylor**[3]

[1] Department of Physics, University of Crete, and Foundation for Research and Technology – Hellas, Heraklion, GR-71409, Crete, Greece
[2] Research School of Physical Sciences and Engineering, Institute of Advanced Studies, Australian National University, Canberra, ACT 0200, Australia
[3] Atmospheric, Oceanic and Planetary Physics, University of Oxford, England

Received: 7 August 1996 / Revised: 25 July 1997 / Accepted: 31 July 1997

Abstract. A one-dimensional atmospheric photochemical model with an altitude grid of about 1.5 km was used to examine the structure of the global mean vertical ozone profile and its night-time-to-daytime variation in the upper atmosphere. Two distinct ozone layers are predicted, separated by a sharp drop in the ozone concentration near the mesopause. This naturally occurring mesopause ozone deep minimum is primarily produced by the rapid increase in the destruction of water vapour, and hence increase in HO_x, at altitudes between 80 and 85 km, a region where water-vapour photodissociation by ultraviolet radiation of the solar Lyman-alpha line is significant, and where the supply of water vapour is maintained by methane oxidation even for very dry conditions at the tropospheric-stratospheric exchange region. The model indicates that the depth of the mesopause ozone minimum is limited by the efficiency with which inactive molecular hydrogen is produced, either by the conversion of atomic hydrogen to molecular hydrogen via one of the reaction channels of H with HO_2, or by Lyman-alpha photodissociation of water vapour via the channel that leads to the production of molecular hydrogen. The ozone concentration rapidly recovers above 85 km due to the rapid increase in O produced by the photodissociation of O_2 by absorption of ultraviolet solar radiation in the Schumann-Runge bands and continuum. Above 90 km, there is a decrease in ozone due to photolysis as the production of ozone through the three-body recombination of O_2 and O becomes slower with decreasing pressure. The model also predicts two peaks in the night-time/daytime ozone ratio, one near 75 km and the other near 110 km, plus a strong peak in the night-time/daytime ratio of OH near 110 km. Recent observational evidence supports the predictions of the model.

Correspondence to: I. M. Vardavas
e-mail: vardavas@iesl.forth.gr

Key words Atmospheric composition and structure · Middle atmosphere · Thermosphere · Transmission and scattering of radiation

1 Introduction

We have examined the role of H_2O photodissociation on ozone concentration in the upper atmosphere with particular emphasis on the region between 70 and 95 km altitude, where we expect water-vapour photodissociation by the solar Lyman-alpha line to be important. As was shown by Lewis *et al.* (1983), the photodestruction rate of water vapour by Lyman-alpha peaks within the layer between 70 and 95 km. We have therefore used a 1D photochemical model with a fine pressure grid (corresponding to intervals of about 1.5 km at these altitudes) in order to isolate processes that might have small characteristic length scales. Our present study is motivated by the wealth of recent satellite concentration data of atmospheric species important to atmospheric ozone photochemistry that are available from such data bases as UARS/HALOE, ISAMS, MLS, ATMOS and SME with ground-based and in situ data avaliable for validation. In this initial study we compare our model predictions with some typical vertical ozone profiles obtained by ATMOS (Atmospheric Trace Molecule Spectroscopy experiment on Spacelab 3) and HALOE (Halogen Occultation Experiment launched on the Upper-Atmospheric Research Satellite, UARS, in September 1991 as part of the Mission to Planet Earth, MTPE, Program). Figures 1 and 2 show typical vertical ozone profiles obtained by HALOE at sunrise and sunset, respectively. Ozone values with altitude are given in the HALOE data base along with a quality factor which represents the statistical error in the measurements. An estimate of the error, taken here to be the quality divided by four (see Overview of HALOE Data Quality Status in the

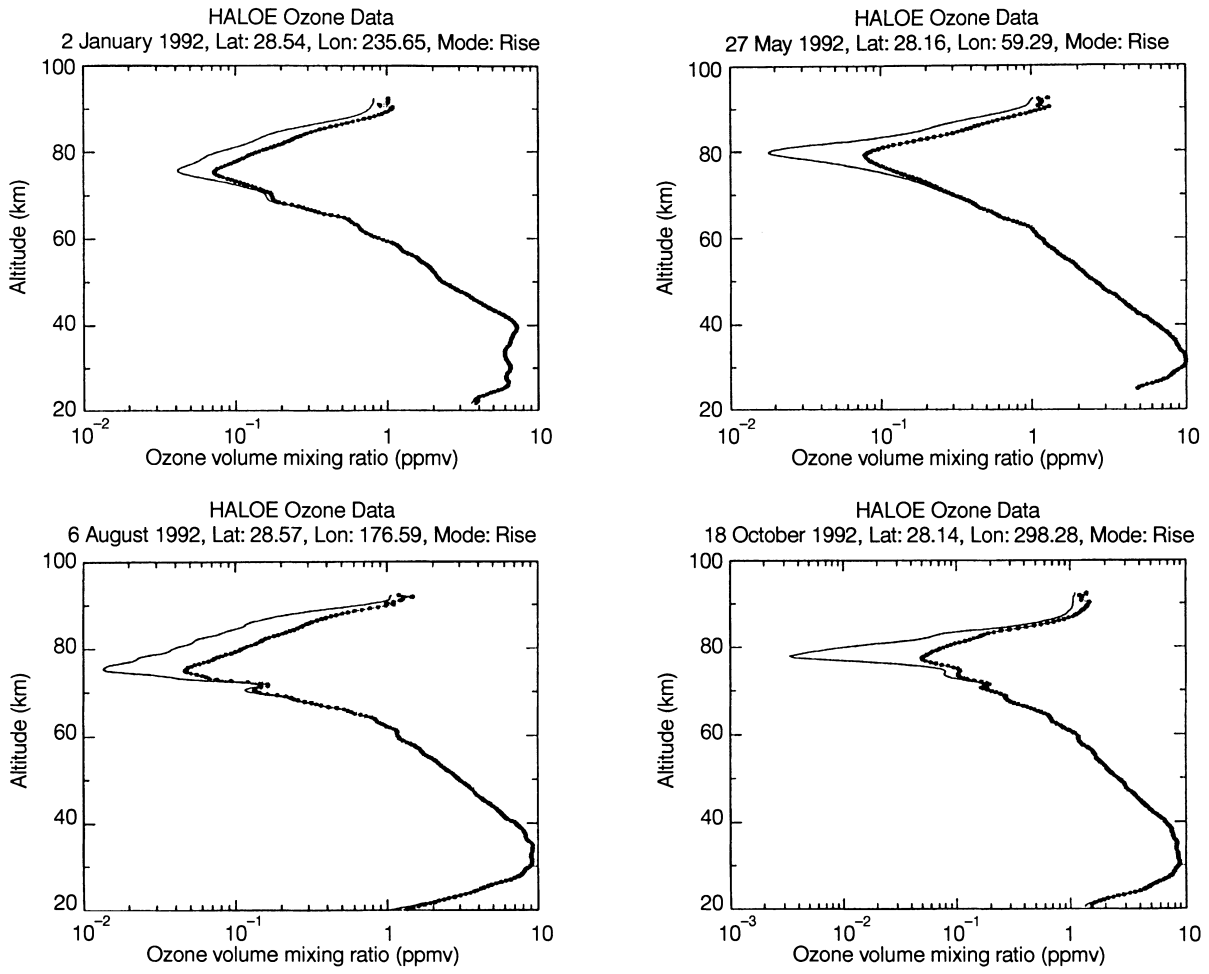

Fig. 1. A sample of HALOE ozone profiles showing mean (*fine line*) and estimated upper limit (*thick line*) profiles at sunrise in the northern hemisphere

data base), gives an indication of the upper limit of the measurements when added to the given mean value. Above 70 km, the estimated upper limit starts to deviate from the mean value. However, both the mean profiles and the estimated upper limit profiles indicate that there is a deep minimum generated near the mesopause. The depth of the minimum is variable with minimum mixing ratios usually below 0.1 ppmv. Our model computations show that the deep mesopause ozone minimum is created by the reaction of ozone with the active hydrogen species HO_x (H, OH and HO_2) that are produced by the photodissociation of water vapour, and that the variability of the depth of the minimum depends on the efficiency of the conversion of H to H_2 through the reaction of H with HO_2, and on the production of molecular hydrogen during Lyman-alpha photodissociation of water vapour.

2 The role of water-vapour photodissociation

The role of the HO_x species (H, OH and HO_2) in destroying ozone near the mesopause was investigated in detail by Allen *et al.* (1984), who stressed the key role played by reactions which convert the active-hydrogen HO_x species to the inactive-hydrogen species H_2 and H_2O. The subsequent reaction rate measurements of Keyser (1986) for the reaction of H with HO_2 and estimates of the branching ratios which lead to either active or inactive hydrogen species highlighted the role of this reaction in controlling ozone concentrations near the mesopause. The reaction of H with HO_2 has three reaction channels (e.g. Keyser, 1986; DeMore *et al.*, 1994)

$$H + HO_2 \rightarrow OH + OH \quad 0.90 \pm 0.04 \ ,$$

$$H + HO_2 \rightarrow O + H_2O \quad 0.02 \pm 0.02$$

and

$$H + HO_2 \rightarrow H_2 + O_2 \quad 0.08 \pm 0.04 \ ,$$

where the first which leads to the production of the active hydrogen species OH is dominant (branching ratio 0.9). It is the strength of the third channel which limits the role of water-vapour photodissociation in ozone reduction through the conversion of atomic hydrogen to inactive molecular hydrogen. According to Keyser's work, the third channel's branching ratio was determined from knowledge of the total reaction rate and the branching ratios of the first two channels.

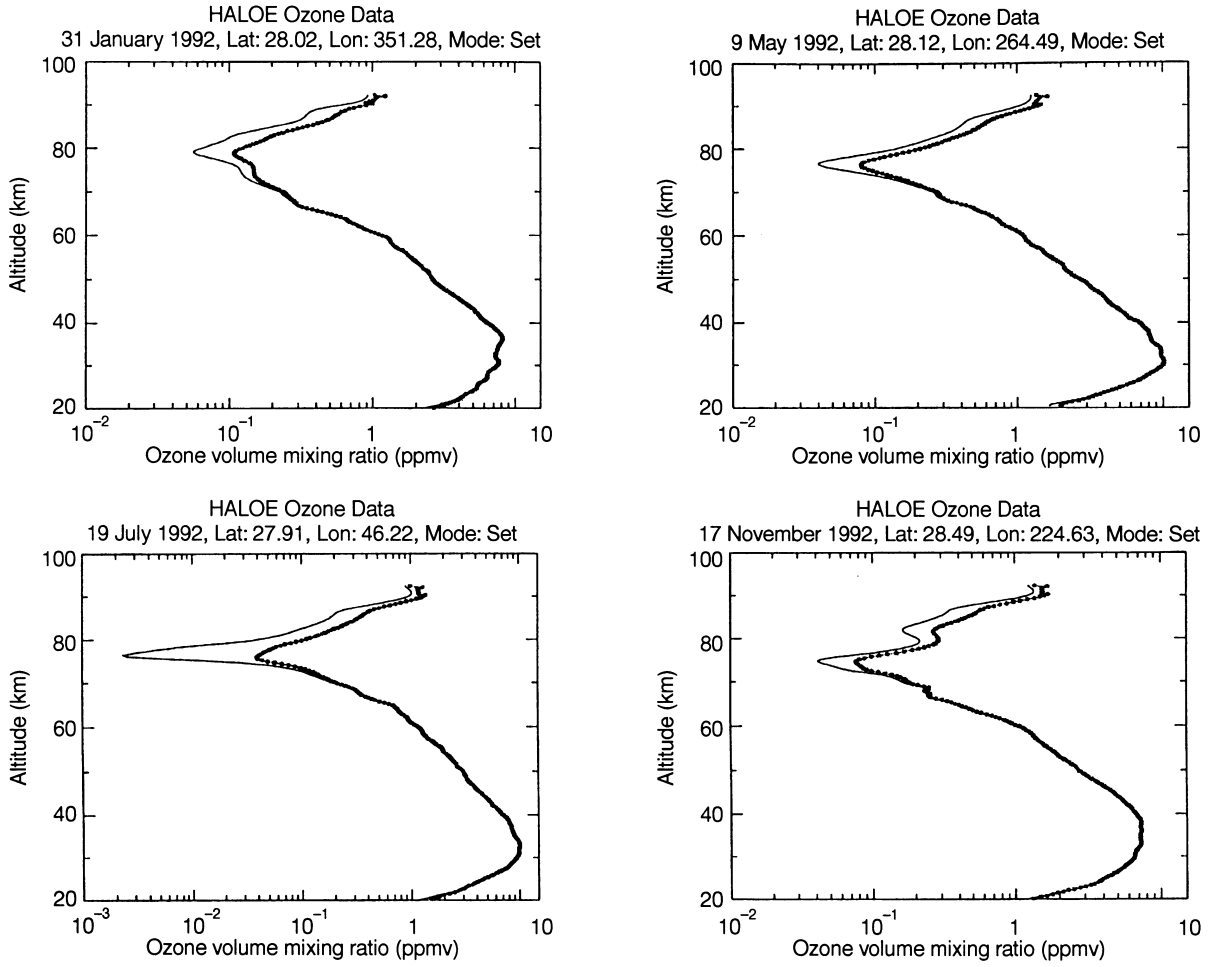

Fig. 2. A sample of HALOE ozone profiles showing mean (*fine line*) and estimated upper limit (*thick line*) profiles at sunset in the northern hemisphere

Given the uncertainties in the branching ratios of the first two channels and the fact that these were determined for the temperature range 245–300 K, Keyser concluded that a more exact study of the third channel and its temperature dependence was warranted, having found no significant temperature dependence for the total reaction rate and branching ratios in this temperature range. Clearly, measurements typical of the low-temperature (below 200 K) conditions near the mesopause are needed.

Photolysis of water vapour by Lyman-alpha can also result in the production of active and inactive hydrogen species. The two channels for the photodissociation of water vapour by Lyman-alpha are

$$H_2O + h\nu \rightarrow H + OH \qquad \alpha$$

$$H_2O + h\nu \rightarrow H_2 + O^1D \qquad 1 - \alpha \ ,$$

where the branching ratio α for the first channel is about 0.75 and for the second about 0.25 according to Stief *et al.* (1972), while according to Banks and Kockarts (1973), the direct production of H_2 from the photodissociation of water vapour is a small fraction of the process of Lyman-alpha photodissociation leading to the production of the HO_x species.

3 The model

The 1D photochemical model used comprises two radiation transfer submodels (Vardavas and Carver, 1984a; Strobel, 1987), a radiative-convective equilibrium submodel (Vardavas and Carver, 1985) and a chemical kinetics-diffusion submodel (Vardavas, 1984; Vardavas *et al.*, 1990). One radiation submodel simulates the transfer of solar visible and near-infrared plus terrestrial infrared flux through the atmosphere. These fluxes are used to compute net heating-cooling in the radiative-convective model which computes the vertical atmospheric temperature profile needed for the computation of reaction rates. Alternatively, one can specify a vertical temperature structure and use the radiative-convective model to compute the radiation fields. The other radiation submodel simulates the atmospheric transfer of solar uv from 0.01 μm to Lyman-beta, to take into account reactions of the ionic species leading to the formation of NO in the lower thermosphere (Siskind and Rusch, 1992), and from Lyman-alpha to 0.35 μm, visible, and near infrared up to 1 μm allowing for pure absorption, Rayleigh and cloud Mie multiple scattering and surface reflection (Vardavas and Koutoulaki, 1995).

The solar flux is used to compute photodissociation rates using 206 wavelength-grid points. The photodissociation rates depend strongly on O_2 uv absorption in the highly structured Schumann-Runge (S-R) bands (Lewis *et al.*, 1994; Allen and Frederick, 1982). The O_2 S-R bands affect both the uv radiation field, and hence the photodissociation rates of other species, and the photodissociation of O_2. The incoming solar flux spectrum profile at the top of the atmosphere is normalized to a solar constant of 1367 Wm^{-2}. The solar zenith angle, cloud cover, and ground albedo are specified.

Reaction and photodissociation rates (DeMore *et al.*, 1994) are used in a system of 182 reactions, to simulate the vertical transport of 53 species based on a semi-empirical expression for vertical eddy diffusion. The diffusion coefficient was taken from Brasseur and Solomon (1984) up to 100 km, while above that the eddy diffusion coefficient was taken to decrease rapidly (e.g. Strobel, 1989; Roble, 1995) and molecular diffusion becomes important. The bi-molecular diffusion coefficients were taken from Vargaftik (1975). Equilibrium vertical profiles of species concentrations were computed using diurnal averaging by computing the daytime and night-time species concentrations (Turco and Whitten, 1978). Near the ground, emission and deposition processes are included (Wuebbles, 1981). Water vapour at the surface and in the troposphere is computed from a specified relative humidity profile and the tropospheric temperature structure.

The model divides the atmosphere into a fine grid of 100 altitude (pressure) levels, to avoid pressure-dependent changes in temperature and composition (Vardavas and Carver, 1984b). Constant-flux boundary conditions are enforced at the top of the atmosphere, and also at the ground for most species rather than fixed concentration boundary conditions, to allow the species concentrations to obtain the values dictated by the photochemical and physical processes. This does not exclude the possibility of specifying a surface flux which can be included through the emission or deposition processes.

The model was used to generate a global mean ozone profile (reflecting mid-latitude conditions) by setting the solar zenith angle to 60°, cloud-cover fraction to 0.5, surface albedo to 0.1 (mostly ocean), a surface relative humidity of 0.8 and the US Standard Atmosphere temperature structure. The chemistry was set to a 1960 standard without CFCs and total Cl_x of 1 ppbv (Johnston *et al.*, 1989).

4 Results

4.1 Diurnally averaged profiles

In Fig. 3 our model results (curve a + b + c) for the diurnally averaged ozone profile computed using the $H + HO_2$ branching ratios of Keyser and a photodissociation branching ratio $\alpha = 1$ are compared with the profile of Roble (1995), which used solar minimum

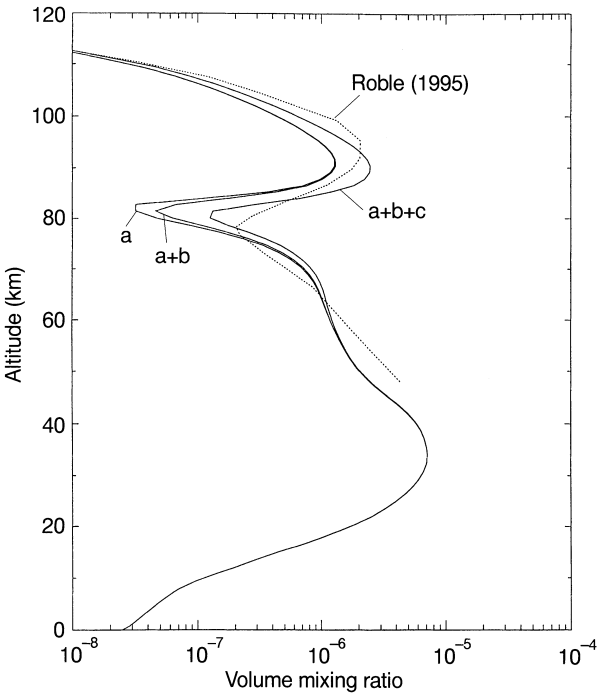

Fig. 3. Model global mean diurnally averaged ozone profiles with and without channels a, b and c of the reaction $H + HO_2$, using a Lyman-alpha water-vapour photodissociation branching ratio $\alpha = 1$

radiation flux conditions and branching ratios taken from Brasseur and Solomon (1986). Computations with the branching ratios given in Roble showed no significant difference from the ozone profile of curve a + b + c. On removing the third channel of the reaction of H and HO_2, the mesopause ozone minimum deepens considerably (curve a + b), while removal also of the second channel leads to a further deepening of the minimum (curve a). Our model's deep minimum, obtained by removing the channels that convert the active H species to inactive molecular hydrogen and water vapour, is in better agreement with the observations.

In Fig. 4 are shown the ozone profiles obtained using all three channels for the reaction of H with HO_2 for different values of the Lyman-alpha photodissociation branching ratio α. The profile with $\alpha = 0$, which corresponds to photodissociation that leads to the production of inactive molecular hydrogen, exhibits a very weak ozone minimum at the mesopause. The profile with $\alpha = 1$, which corresponds to photodissociation that leads to the production of active atomic hydrogen, exhibits a deep minimum in ozone concentration at the mesopause. Clearly the reactions that produce molecular hydrogen instead of active atomic hydrogen limit the depth of the ozone minimum at the mesopause.

Our model shows a strong rise in the H concentration near the mesopause, rising to a value of 1.3×10^{-5} ppmv, in keeping with other models (Strobel, 1972; Brasseur and Solomon, 1984) and gives an H escape rate of 2.8×10^8 molecules/cm^2s, close to the estimates of others (Carver, 1981; Kasting *et al.*, 1979). Our model H_2O profile, obtained using a global mean surface

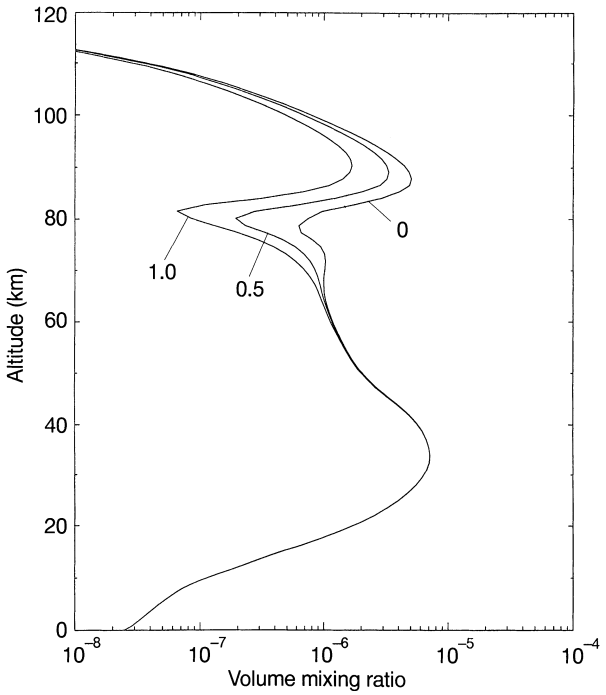

Fig. 4. Model global mean diurnally averaged ozone profiles for different values of the branching ratio α for the photodissociation of water vapour by Lyman-alpha, using the branching ratios of Keyser (1986) for the reaction $H + HO_2$

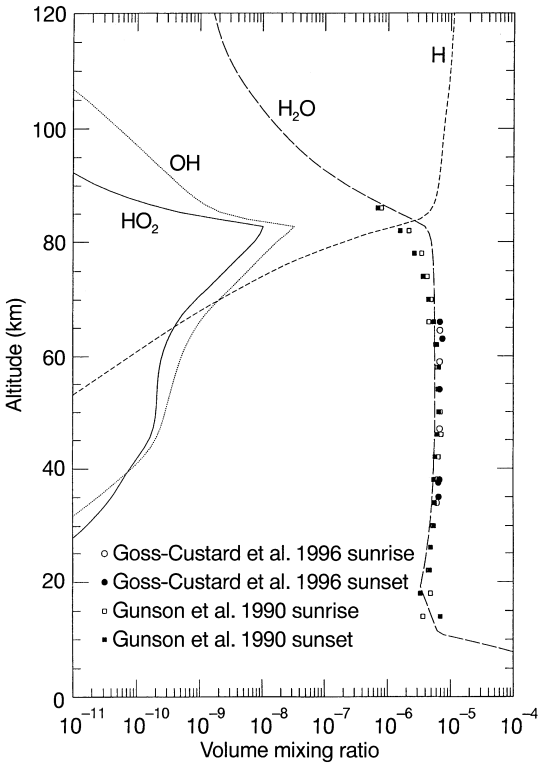

Fig. 5. Model diurnally averaged volume mixing ratio for HO_x and H_2O together with sunrise and sunset H_2O UARS/ISAMS measurements given in Goss-Custard *et al.* (1996) and the ATMOS measurements given in Gunson *et al.* (1990)

relative humidity value of 0.8, is in very good agreement with the ATMOS observations given in Gunson *et al.* (1990) and with the UARS/ISAMS observations given in Goss-Custard *et al.* (1996), as shown in Fig. 5.

Figure 6 shows the ozone profiles obtained for different water-vapour profiles for progressively drier tropopause conditions obtained by setting the surface relative humidity equal to 0.8, 0.4 and 0.1, using channel a only for the reaction of $H + HO_2$ and $\alpha = 1$. The water vapour mixing ratio in the stratosphere and mesosphere is maintained by methane oxidation even for very dry conditions in the tropospheric-stratospheric exchange region. The corresponding mesopause ozone deep minimum is thus made slightly shallower by the drop in the water-vapour mixing ratio whose peak value in the upper atmosphere goes from 5.7 to 2.9 ppmv, when the surface relative humidity is reduced from 0.8 to 0.1.

4.2 Night-time/daytime ratios

In Fig. 7 are given the daytime and night-time model profiles for the channel-a-only case with $\alpha = 1$, and these are compared with: the ATMOS sunrise and sunset observations (Gunson *et al.*, 1990) at two locations – 48°S (sunrise) and 28°N (sunset) – from 30 April through 6 May 1985; and with the HALOE observations in May 1992 at 49°S (sunrise) and 28°N (sunset). Both the sunset and sunrise observations below 80 km follow more closely the daytime values of the model, while above 80 km both observation sets exhibit the rapid rise in ozone concentration predicted by the model.

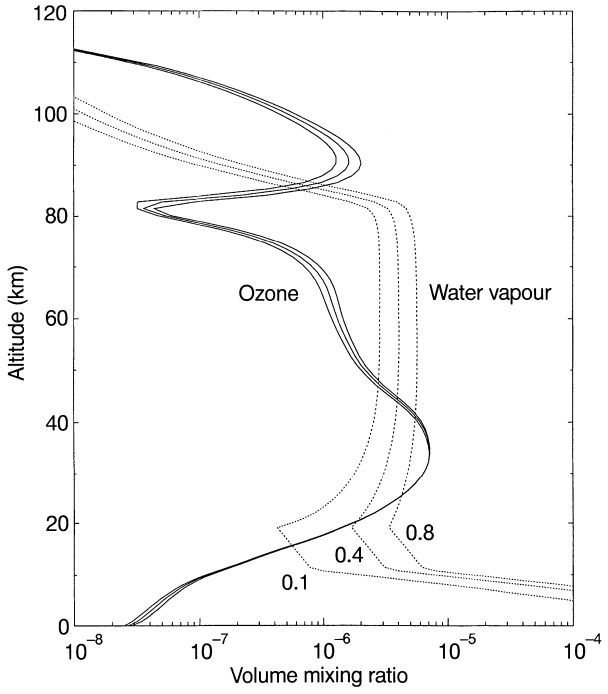

Fig. 6. Model global mean diurnally averaged ozone profiles for different water-vapour profiles computed by setting the surface relative humidity equal to 0.8, 0.4 and 0.1, using channel a only for the reaction $H + HO_2$ and $\alpha = 1$

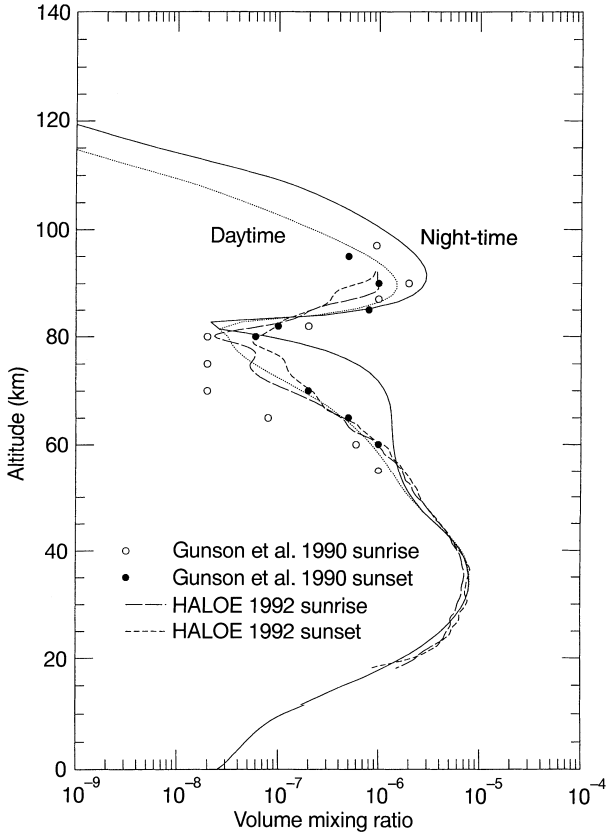

Fig. 7. Global mean daytime and night-time averaged ozone profiles computed by the model are compared with the sunrise and sunset measurements obtained by the ATMOS experiment on Spacelab 3 as given in Gunson *et al.* (1990) and by UARS/HALOE

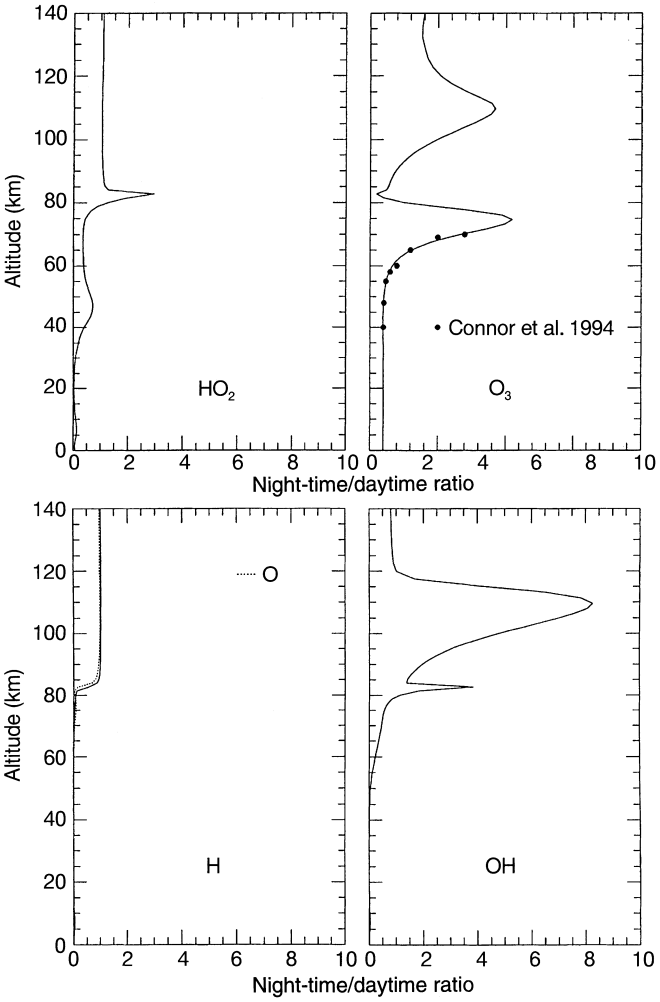

Fig. 8. Model night-time/daytime ratios for the HO_x species and for O_3. *Solid circles* are the ground-based microwave O_3 ratio observations of Connor *et al.* (1994)

The night-time-to-daytime variation of the ozone concentration generated by the model is in agreement with the mid-latitude variation (with a weak seasonal dependence) observed by Connor *et al.* (1994). The ozone night-time/daytime concentration ratio predicted by the model is given in Fig. 8, along with the corresponding ratios for the HO_x species and O. The ratio for ozone is in very good agreement with the observations up to 70 km, with the night-time mixing ratio remaining nearly constant at about 1.5 ppmv between 60 and 70 km, also in agreement with the observations. The model predicts two distinct peaks in the ozone night-time/daytime ratio, one near 75 km and another near 110 km, plus a sharp narrow dip at about 82 km, which corresponds to a region where the night-time/daytime ratios of OH and HO_2 exhibit very sharp peaks, resulting in more effective night-time destruction of ozone by these two species.

5 Discussion

Our interpretation of the strong ozone reduction in the mesopause region and of the night-time/daytime ratios is as follows.

In the stratosphere below about 50 km, the destruction of ozone is balanced by three-body recombination of O and O_2, so that the equilibrium that is rapidly maintained during daytime is unaltered at night-time. Note that the night-time/daytime ratio for O is negligible up to about 70 km.

Between 50 and 70 km, direct photolysis of ozone in the Hartley-Huggins bands reduces the ozone daytime concentration, while the night-time mixing ratio is maintained fairly constant with altitude (Fig. 7) through (eddy) diffusive equilibrium with the atmospheric layers from below. The result is a rise in the night-time/daytime concentration ratio of ozone as shown in Fig. 8. There is also some rise in the night-time concentration of HO_2 due to photodissociation shielding at night-time (Fig. 8). Above 60 km, there is a rapid rise in daytime H with altitude through the photodissociation of water vapour by Lyman-alpha and ultraviolet radiation in the region of the Schumann-Runge bands of oxygen. This is accompanied by a rise in the daytime concentration of the other HO_x species, OH and HO_2.

Between 70 and 80 km, there is a rise in night-time H accompanied by an increase in the other HO_x species, as diffusion from above rises the H night-time/daytime ratio towards unity, which occurs at about 85 km. This results in a decrease in the night-time/daytime ratio of

ozone between 70 and 80 km. The very rapid rise in night-time H between 80 and 85 km results in a rapid rise in night-time OH and HO_2, as the latter is shielded at night from photodissociation, with an associated sharp drop in the night-time/daytime ozone ratio below unity. In this region, atomic oxygen rises rapidly due to the photodissociation of molecular oxygen by absorption of solar ultraviolet radiation by the Schumann-Runge bands and continuum. As in the case of H, through diffusion from above, the night-time/daytime ratio of O rapidly rises to unity at about 85 km. This results in two processes.

First, the rapid rise in O between 80 and 90 km produces a rapid rise in ozone concentration both during daytime and night-time (Fig. 7), sufficient to counteract the effects of the decreased production of ozone with altitude via the pressure-dependent three-body recombination of O and O_2. Above 90 km, there is a rapid decrease in daytime ozone with altitude due to photolysis, accompanied by a drop in night-time ozone, as the fall in pressure results in a decrease in the rate of ozone production via the three-body recombination of O and O_2.

Photolysis produces a rise in the night-time/daytime ozone ratio, with a peak at about 110 km, as shown in Fig. 8. Secondly, since HO_2 in this region is created by three-body recombination of H and O_2 and is destroyed by reaction with O, and both H and O have night-time/daytime ratios of unity above about 85 km, the night-time/daytime ratio of HO_2 also falls to unity. The drop in the night-time/daytime ratio of HO_2 initially produces a drop in the ratio of OH, but this is followed by a rise in the night-time/daytime ratio of OH as ozone reacts with H to produce OH in this region. The OH night-time/daytime ratio therefore follows the variation in the ozone night-time/daytime ratio.

We have performed some preliminary sensitivity tests to evaluate the response of the ozone deep minimum near the mesopause to changes in some of the atmospheric properties. Reduction of the reaction rate constant for the reaction of HO_2 with O to produce OH and O_2 by 70% of its JPL94 value (DeMore *et al.*, 1994), as proposed by Clancy *et al.* (1994), did not change the structure of the minimum and second ozone layer, but did increase the ozone concentration in the layers from 40 to 70 km, in keeping with their results. We have also made a preliminary examination of the effect of the thermospheric rise in temperature on the ozone concentration and night-time/daytime ratio profiles by setting the temperature equal to the minimum mesopause value of 186 K. The effect was to remove the second peak in the ozone night-time/daytime ratio near 110 km and to replace it by a continuous rise from about 100 km. The thermospheric rise in NO was also found not to affect significantly the structure of the second ozone layer. Variation of the ozone mesopause minimum between solar cycle minimum and maximum [using a uv flux variation from Vardavas (1987)] was found to be weak, although both the stratospheric and lower thermospheric peaks in ozone concentration were found to be enhanced at solar maximum as expected.

6 Summary

Our model computations indicate that there are two distinct ozone layers in the atmosphere, separated by a sharp drop in the ozone concentration near the mesopause. The depth of the mesopause ozone minimum is limited by the efficiency with which inactive molecular hydrogen is produced, either by the conversion of atomic hydrogen to molecular hydrogen via one of the reaction channels of H with HO_2 or by Lyman-alpha photodissociation of water vapour via the channel that leads to the production of molecular hydrogen. Recent satellite observations exhibit this deep minimum in mesopause ozone. Both laboratory reaction rates between H and HO_2 at low temperatures and more accurate ozone measurements above 80 km are required better to quantify the depth of the minimum and its variation.

Acknowledgements. This research project was supported by a NATO Collaborative Research Grant (CRG 940950).

Topical Editor F. Vial thanks two referees for their help in evaluating this paper.

References

Allen, M., and J. E. Frederick, Effective photodissociation cross sections for molecular oxygen and nitric oxide in the Schumann-Runge bands, *J. Atmos. Sci.*, **39,** 2066–2075, 1982.

Allen, M., J. I. Lunine, and Y. L. Yung, The vertical distribution of ozone in the mesosphere and lower atmosphere, *J. Geophys. Res.*, **89,** 4841–4872, 1984.

Banks, P. M., and G. Kockarts, *Aeronomy*, *Part A*, Academic Press, New York, 1973.

Brasseur, G. M., and S. Solomon, *Aeronomy of the middle atmosphere*, D. Reidel, Norwell, Mass., 1984.

Carver, J. H., Prebiotic atmospheric oxygen levels, *Nature*, **292,** 136–138, 1981.

Clancy, R. T., B. J. Sandor, D. W. Rusch, and D. O. Muhleman, Microwave observations and modeling of O_3, H_2O and HO_2 in the mesosphere, *J. Geophys. Res.* **99,** 5465–5473, 1994.

Connor, B. J., D. E. Siskind, J. J. Tsou, A. Parish, and E. E. Remsberg, Ground-based microwave observations of ozone in the upper stratosphere and mesosphere, *J. Geophys. Res.*, **99,** 16757–16770, 1994.

DeMore, W. B., S. P. Sander, D. M. Golden, R. F. Hampson, M. J. Kurylo, C. J. Howard, A. R. Ravishankara, C. E. Kolb, and M. J. Molina, *Chemical kinetics and photochemical data for use in stratospheric modelling*, JPL Publ. 94-20, Pasadena, 1994.

Goss-Custard, M. A., J. J. Remedios, A. Lambert, F. W. Taylor, C. D. Rodgers, M. Lopez-Puertas, G. Zaragoza, M. R. Gunson, M. R. Suttie, J. E. Harries, and J. M. Russell III, Measurements of water vapour distributions by the improved stratospheric and mesospheric sounder: Retrieval and validation, *J. Geophys. Res.*, **101,** 9907–9928, 1996.

Gunson, M. R., C. B. Farmer, N. R. Norton, R. Zander, C. P. Rinsland, J. H. Shaw, and B. C. Gao, Measurements of CH_4, N_2O, CO, H_2O, and O_3 in the middle atmosphere by the Atmospheric Trace Molecule Spectroscopy Experiment on Spacelab 3, *J. Geophys. Res.*, **95,** 13867–13882, 1990.

Johnston, H. S., D. E. Kinnison, and D. J. Wuebbles, Nitrogen oxides from high-altitude aircraft: an update of potential effects on ozone, *J. Geophys. Res.*, **94,** 16351–16363, 1989.

Kasting, J. F., S. C. Liu, and T. M. Donahue, Oxygen levels in the prebiological atmosphere, *J. Geophys. Res.*, **84,** 3097–3107, 1979.

Keyser, L. F., Absolute rate constant and branching fractions for the $H + HO_2$ reaction from 240–300 K, *J. Phys. Chem.*, **90,** 2994–3003, 1986.

Lewis, B. R., I. M. Vardavas, and J. H. Carver, The aeronomic dissociation of water vapor by solar H Lyman α radiation, *J. Geophys. Res.*, **88,** 4935–4940, 1983.

Lewis, B. R., S. T. Gibson, and P. M. Dooley, Fine-structure dependence of predissociation linewidth in the Schumann-Runge bands of molecular oxygen, *J. Chem. Phys.*, **100,** 7012–7035, 1994.

Roble, R. G., Energetics of the mesosphere and thermosphere, in *The upper mesosphere and lower thermosphere: a review of experiment and theory*, Eds. R. M. Johnson, and T. L. Killeen, Geophysical Monograph 87, AGU, pp. 1–21, 1995.

Siskind, D. E., and D. W. Rusch, Nitric oxide in the middle to upper thermosphere, *J. Geophys. Res.*, **97,** 3209–3217, 1992.

Stief, L. J., B. Donn, S. Glicker, E. P. Gentieu, and J. E. Mentall, Photochemistry and lifetimes of interstellar molecules, *Astrophys. J.*, **171,** 21–30, 1972.

Strobel, D. F., Minor neutral constituents in the mesosphere and lower thermosphere, *Radio Sci.*, **7,** 1–21, 1972.

Strobel, D. F., Radiative heating-cooling and the energetics of the stratosphere and mesosphere, *Rev. Geophys.*, **25,** 497–500, 1987.

Strobel, D. F., Constaints on gravity-wave induced diffusion in the middle atmosphere, *PAGEOPH*, **130,** 533–546, 1989.

Turco, R. P., and R. C. Whitten, A note on the diurnal averaging of aeronomical models, *J. Atmos. Terr. Phys.* **40,** 13–20, 1978.

Vardavas, I. M., Modelling reactive gas flows within shock tunnels, *Aust. J. Phys.*, **37,** 1–21, 1984.

Vardavas, I. M., Atmospheric temperature response to solar cycle uv flux variations, *Solar Phys.*, **108,** 403–410, 1987.

Vardavas, I.M., and J. H. Carver, Solar and terrestrial parameterizations for radiative-convective models, *Planet. Space Sci.*, **32,** 1307–1325, 1984a.

Vardavas, I.M., and J. H. Carver, Comments on the Newton-Raphson method for obtaining temperature profiles from radiative-convective models, *Planet. Space Sci.*, **32,** 803–807, 1984b.

Vardavas, I. M., and J. H. Carver, Atmospheric temperature response to variations in CO_2 concentration and the solar-constant, *Planet. Space Sci.*, **33,** 1187–1207, 1985.

Vardavas, I.M., and K. Koutoulaki, A model for the solar radiation budget of the northern hemisphere: Comparison with Earth Radiation Budget Experiment data *J. Geophys. Res.*, **100,** 7303–7314, 1995.

Vardavas, I. M., L. M. Cannon, and K. R. Ryan, *BOEING-CSIRO joint research effort, ozone studies project, Tech. Rep. 2*, CSIRO Division of Applied Physics, Sydney, Australia, 1990.

Vargaftik, N. B., *Tables on the Thermophysical Properties of Liquids and Gases*, Wiley, New York, 1975.

Wuebbles, D.J., *A summary of the LLNL one-dimensional transport-kinetics model of the troposphere and stratosphere UCID-19185*, Lawrence Livermore National Laboratory, Livermore, 1981.